Magnetic fabrics in fault-related fold and its relation with finite strain: an example from Mingjiang thrust structures in Western Sichuan*

Jia Dong**, Chen Zhuxin, Luo Liang, Hu Qianwei and Jia Qiupeng

(Department of Earth Sciences, Nanjing University, Nanjing 210093, China)

Accepted on October 13, 2006

Abstract The anisotropy of magnetic susceptibility (AMS) is a quick, effective and sensitive technique used to measure the weakly deformed sedimentary rocks, and also a reliable method to reveal the deforming mechanisms of fault-related folds. In Longmenshan front belt, a typical cross-section of fault-related folds is chosen to study the AMS. A total of 224 oriented specimens have been drilled at 23 different sampling sites which were distributed at the key structural positions of this structural section developed in the Xujiahe formation of the upper Triassic. Six elementary types of magnetic fabrics are recognized and established through this AMS study: 1) a sedimentary fabric; 2) an initial deformation fabric; 3) a pencil structure fabric; 4) a weak cleavage fabric; 5) a strong cleavage fabric; 6) a stretching lineation fabric. It has been found that most of magnetic fabrics are characterized by fabrics of weak deformation which belong to the pure-shear results of a pre-folding layer parallel shortening (LPS). In the fault-bend fold, almost all magnetic fabrics are the initial deformation fabrics of weak deformation, and denote that the deformation in the forelimb is stronger than that in the backlimb and no finite strain is shown in the footwall. While in the fault-propagation fold, finite strains are concentrated in the trishear zone where magnetic fabric results are approximately consistent with the estimated consequences of the kinematic model. The tectonic stress field indicated by the magnetic fabrics is basically the same along the whole structural section and shows a NW to SE compression and shortening which is accordant with the regional compressive stress field of the Longmenshan fold-thrust belt.

Keywords: magnetic fabric, finite strain, fault-related fold, trishear zone, Longmenshan.

The fold-and-thrust belt is a transition zone between an apparently undeformed foreland and an orogenic belt characterised by high strain and metamorphism, where sedimentary beds are folded and faulted but rocks do not show evidence of strong internal deformation (strain). Nevertheless, it has been confirmed that anisotropy of magnetic susceptibility (AMS) as a special magnetic fabric can record the cryptic deformation caused by pure or simple shear in sedimentary rocks from fold-and-thrust belts[1—3]. As we have known, there are several mechanisms of fault-related folding such as kink-band model, limb-rotation model, trishear model, etc.[4—6], which may cause different strain distributions in the folded rocks. At present, the geometric modeling is the common method to deduce the kinematic processes and mechanisms of the fault-related folds. However, the folding process includes the body translation, body rotation and internal deformation, and is controlled by the complicated and unclear combination of these factors[7]. Some scholars[8—10] speculated that the internal strain may be small in large-displacement thrusting nappes, while the remarkable strain may be developed in the less displacement ones. So the kinematic analyses of the fold-thrust structures should be based on the combination of balanced cross-section and finite strain[11]. The AMS investigation in the deformed sedimentary rocks may be a reliable and effective method to reveal the mechanisms of fault-related folding. This paper reports on the AMS investigation along a section across the Longmenshan front belt and aims to discuss the finite strain characteristics in the fault-related fold through magnetic fabric analyses.

1 Geological setting and sampling

The Longmenshan is one of the typical foreland fold-thrust belts in western China[12—14] and comprises a series of thrusting nappes and thrust sheets from NW to SE[15—17]. Across the Longmenshan front belt, we chose Mingjiang cross section of fault-related folds in Dujiangyan area for this AMS investigation (Fig. 1a).

* Supported by the National Natural Science Foundation of China (Grant Nos. 40372091 and 40672132)

** To whom correspondence should be addressed. E-mail: djia@nju.edu.cn

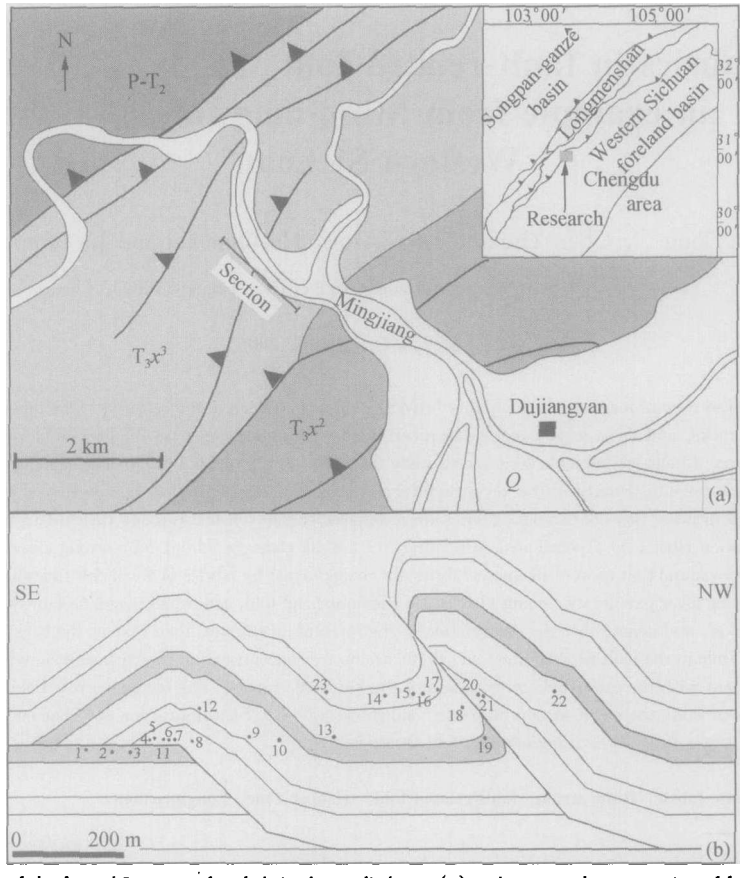

Fig. 1. Geological map of the frontal Longmenshan belt in the studied area (a) and structural cross-section of fault-related folds and sampled sites (b).

Along Mingjiang valley, two typical fault-related folds developed in the third member of Xujiahe formation of the upper Triassic (T_3x^3). Baisha anticline locating at the southeastern part of this section is characterized by the fault-bend fold and presents an outcrop of a hanging wall ramp at the core of anticline. The dip angle of the forelimb is 40°—50° and the backlimb is 20°—35°. Bianbaigou anticline locating at the northwestern part of this structural section is a trishear fault-propagation fold with a vertical or somewhat overturned forelimb, an obviously thickened footwall, and several dip domains separated by axial surfaces in the backlimb (Fig. 1b). By using Trishear 4.5, forward modeling was simultaneously conducted to validate the reasonableness and balance of this fault-related fold cross section. At the extended strike direction of these fault-related folds, we have recognized growth strata of near top Cretaceous and Paleogene and an unconformity of Neogene, which indicates that these folds were developed during latest Cretaceous to early Cenozoic[18].

The whole structural section is composed of the third member of Xujiahe formation of the upper Triassic which shows fluvial and lacustrine sedimentary rocks of medium sands, packsands, siltstones, pelitic siltstones and some coal seams. Along two parallel roads (about 50—60 meters apart in height) within this section, with a special drilling machine for Palaeomagnetism, 224 oriented specimens were drilled in 23 different sampling sites which are distributed at the key structural positions of the folds. All specimens were drilled from the third member of Xujiahe formation, and each of them is 22 mm long and has a diameter of 25.4 mm.

2 AMS results

In order to ascertain the main magnetic carrier minerals, we selected five specimens to conduct experiments of the demagnetization of three orthogonal isothermal remanent magnetization (IRM) and IRM acquisition. A representative result is shown in Fig. 2. In the stepwise demagnetization of IRM, hard, medium and soft coercivities range in windows 0.4 T < hard < 2.2 T, 0.15 T < medium < 0.4 T and

soft < 0.15T, respectively. The soft fractions of coercivities dominate the minerals with a maximum blocking temperature of 580℃, which means that the magnetite is the main magnetic carrier mineral (Fig.2 (a)). This result is supported by IRM acquisition where saturation is quickly approached at the outset of the experiment for a 300 mT applied field (Fig. 2 (b)).

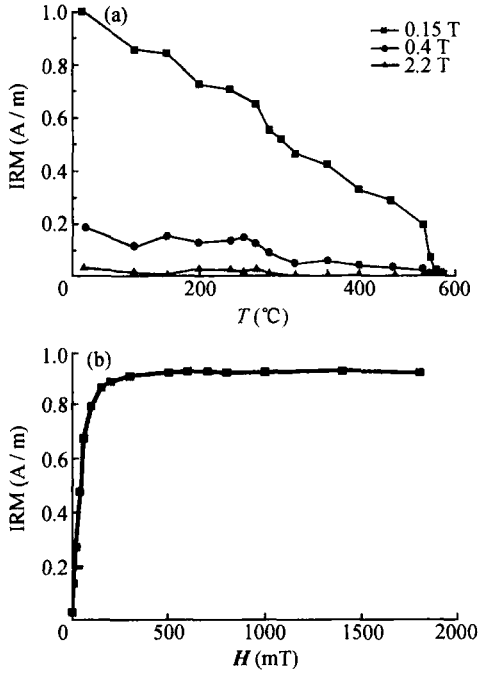

Fig. 2. Representative example of IRM demagnetisation curves (a) and IRM acquisition curve (b). H: applied field strength.

A total of 224 specimens were measured for AMS fabrics. The AMS was measured using a KLY—3 Kappabridge susceptibility instrument located at Institute of Geomechanics of Chinese Academy of Geological Sciences, Beijing. Each specimen was measured twice in three positions and the AMS results are compiled in Table 1. The bulk susceptibilities of all specimens range from 74.63×10^{-6} to 613.3×10^{-6} SI and have a mean bulk magnetic susceptibility of 213.5×10^{-6} SI, which indicates a very low magnetic susceptibility range for the sedimentary rocks. Magnetic fabric may be visualized as an ellipsoid with orthogonal principal axes $K_1 \geqslant K_2 \geqslant K_3$. Basic elements of a magnetic fabric are the magnetic foliation (plane $K_1 - K_2$) and the magnetic lineation (K_1) when they are statistically defined. Both magnetic foliation and lineation are related to petrofabrics[19—21]. In Flinn diagram for magnetic fabric, most of sampling sites are located in the area below straight line $E = 1$ and only site 16, 19, 21 located on that line (Fig. 3a). This behavior means that the shape of the AMS ellipsoid is generally oblate ($L = 1.004 \pm 0.003 < F = 1.015 \pm 0.012$). The shape of the AMS ellipsoid can also be shown in a P' vs. T diagram[22] (Fig. 3(b)), where T reflects the shape of the AMS ellipsoid and P' means the degree of anisotropy. The shape of the magnetic fabric is essentially oblate while only three sites (16, 19 and 21) have a prolate fabric. P' ranges from low values of 1.0079 up to 1.043. The mean value of P' ($P' = 1.022 \pm 0.015$) is typical of weakly deformed rocks[19]. It can be concluded that the fault-related fold shows no obvious control on the distribution of these AMS parameters in this section. As sedimentary rocks progressively deformed, the evolution of the magnetic fabric is firstly from oblate (sedimentary) to prolate and then comes back to oblate (structural). Because of the rapid transition between oblate and prolate, both Flinn and Jelinek plot are difficult to distinguish the different evolution period of the AMS ellipsoids[19,23].

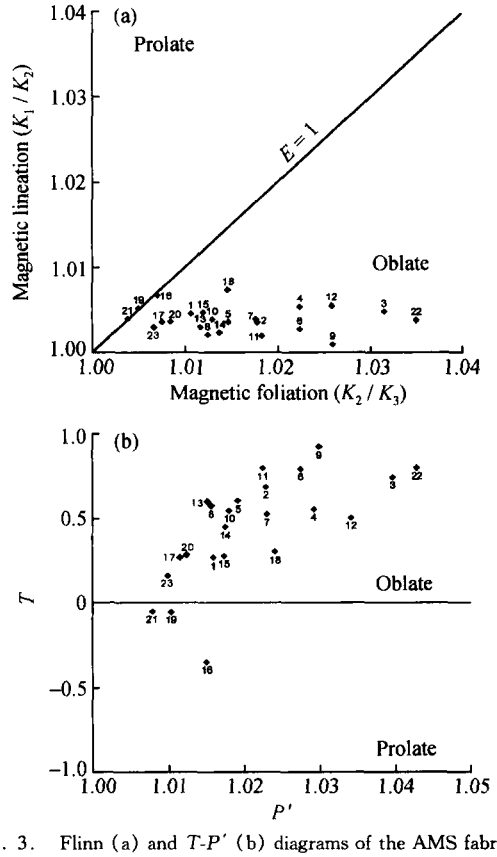

Fig. 3. Flinn (a) and T-P' (b) diagrams of the AMS fabrics.

Table 1. Summary of AMS results in Mingjiang cross section of fault-related fold

SN	Site	North latitude	East longitude	n	$K_m(\times 10^{-6})$	L	F	P'	T
1	bs01	31°01.082′	103°34.962′	11	175.2	1.0045	1.0106	1.0160	0.2707
2	bbs01	31°01.066′	103°34.946′	9	213.66	1.0036	1.0178	1.0230	0.6901
3	bbs02	31°01.068′	103°34.927′	5	324.74	1.0048	1.0314	1.0398	0.7470
4	bs04	31°01.066′	103°34.919′	11	205.6	1.0054	1.0224	1.0294	0.5587
5	bs05	31°01.069′	103°34.909′	8	223.8	1.0036	1.0146	1.0193	0.6069
6	bs06	31°01.073′	103°34.895′	12	232.6	1.0028	1.0223	1.0276	0.7977
7	bs07	31°01.074′	103°34.89′	12	251.8	1.0039	1.0176	1.0231	0.5269
8	bs08	31°01.081′	103°34.881′	11	175.4	1.0021	1.0124	1.0157	0.5771
9	bs09	31°01.102′	103°34.847′	7	220.1	1.0010	1.0258	1.0300	0.9280
10	bs10	31°01.118′	103°34.818′	12	151.1	1.0039	1.0129	1.0181	0.5509
11	bbs03	31°01.065′	103°34.903′	11	252.41	1.0020	1.0183	1.0225	0.8005
12	bs23	31°01.061′	103°34.857′	4	74.63	1.0055	1.0258	1.0343	0.5083
13	bbs04	31°01.139′	103°34.778′	12	178.47	1.0030	1.0116	1.0153	0.6036
14	bbs08	31°01.134′	103°34.691′	10	169.31	1.0024	1.0137	1.0176	0.4510
15	bs20	31°01.144′	103°34.666′	12	154.6	1.0047	1.0119	1.0175	0.2812
16	bbs07	31°01.142′	103°34.665′	8	115.49	1.0067	1.0070	1.0151	−0.3461
17	bbs06	31°01.155′	103°34.625′	7	128.28	1.0036	1.0075	1.0116	0.2715
18	bs17	31°01.173′	103°34.547′	10	613.3	1.0073	1.0146	1.0242	0.3045
19	bs11	31°01.205′	103°34.648′	10	151.3	1.0052	1.0050	1.0104	−0.0522
20	bbs05	31°01.177′	103°34.536′	10	214.33	1.0037	1.0084	1.0125	0.2849
21	bs16	31°01.183′	103°34.534′	10	192.6	1.0040	1.0038	1.0079	−0.0471
22	bs15	31°01.275′	103°34.473′	12	261.9	1.0038	1.0349	1.0430	0.8042
23	bs22	31°01.080′	103°34.783	10	279.0	1.0029	1.0066	1.0101	0.1725

n: number of specimens; K_m: mean bulk magnetic susceptibility of site; lineation parameter $L = K_1/K_2$; foliation parameter $F = K_2/K_3$; shape parameter $T = (2\eta_2 - \eta_1 - \eta_3)/(\eta_1 - \eta_3)$, where $\eta_1 = \ln K_1$, $\eta_2 = \ln K_2$, $\eta_3 = \ln K_3$, $\eta_m = (\eta_1 + \eta_2 + \eta_3)/3$; degree of anisotropy $P' = \exp\{\mathrm{sqr}[2 \times ((\eta_1 - \eta_m)^2 + (\eta_2 - \eta_m)^2 + (\eta_3 - \eta_m)^2)]\}$.

3 Magnetic fabric types and finite strain

Based on the relationship between magnetic fabrics and finite strain[23—25], the types and developing sequence of the deformation fabrics in sedimentary rocks[7], six elementary types of magnetic fabrics are recognized and established in this fault-related fold cross section (Fig.4). (1) Sedimentary fabric, characterized by bedding normal K_3 and bedding parallel magnetic foliation with disorderly scattered K_1 and K_2, is the result of bedding parallel sedimentation and compaction of slaty and flaky minerals (e.g., muscovite) in stable hydrodynamic environment. In this structural section, sedimentary fabrics (sites 1, 2, 3) are localized in the undeformed rocks of the footwall of the fault-bend fold (Baisha anticline). (2) Initial deformation fabric, a low strain fabric developing in the early phase of structural deformation results in the Y-directing linear orientation of needle shaped minerals for the reason of layer parallel shortening. And in this magnetic fabric, K_3 is still normal to the bedding, and magnetic foliation parallels to the bedding where K_1 concentrates in strike direction of the fold (Y-direction) and K_2 in the dip direction. More than fifty percent of the total sampling sites (e.g., sites 4, 5, 6, 7, 8, 9, 10, 11, 12, 13, 16, 20, 21, 22) show initial deformation fabrics, which are mainly distributed in the fault-bend fold and the backlimb of the fault-propagation fold. (3) Pencil structure fabric, a strong fabric, represents a prolate deformation ellipsoid as a result of mineral rotation in sedimentary rocks which usually underwent a tectonic shortening of 10% to 25%. This fabric has a well-shaped magnetic lineation while lack of magnetic foliation. In this situation, K_1 gets together in the strike direction of the fold, and K_3 disperses in the tectonic shorting direction and well shows the orientation of the maximum regional compressing stress. The representative pencil structure fabric is shown in two sites (14, 15) which only appear at the strongly deformed positions in the fault-propagation fold. (4) Weak cleavage fabric, characterized by Z-direction concentration of K_3 and bedding oblique magnetic foliation with K_1 getting together in the strike direction (Y-direction), denotes a rotation of minerals in sedimentary rocks (maybe new growth of phyllosillicate minerals) when tectonic shortening increases in Z-direc-

tion and elongation in X-direction. Site 19 locating at the overturned rocks in the forelimb of fault-propagation fold is the only one having the weak cleavage fabric. (5) Strong cleavage fabric, appearing when tectonic strain is in great strength which forms cross-cutting planar cleavages, usually filled with nonlinear distributed slaty and needle minerals. So the magnetic foliation transects the bedding, K_3 parallels to the structural Z-direction and K_1 gradually turns to X-direction from Y-direction with the increasing deformation. Site 23 is a typical example of this fabric and site 18 is a less one with Z-direction parallel K_3 and a nearly vertical magnetic foliation but oblique to bedding with a low angle. (6) Stretching lineation fabric, in which K_1 concentrates in the X-direction, K_2 turns to the Y-direction and magnetic foliation still normal to the bedding, is the product of greatly enhanced deformation which causes the concentration of stretching lineation in X-direction on cleavage planes. At site 17, K_1 obviously gathers in X-direction forming well defined stretching lineation, K_2 and K_3 disperse on the bedding, and no regular magnetic foliation appears. We do not clearly understand the structural significance of magnetic fabric behaviours of site 17, which needs further verification and confirmation.

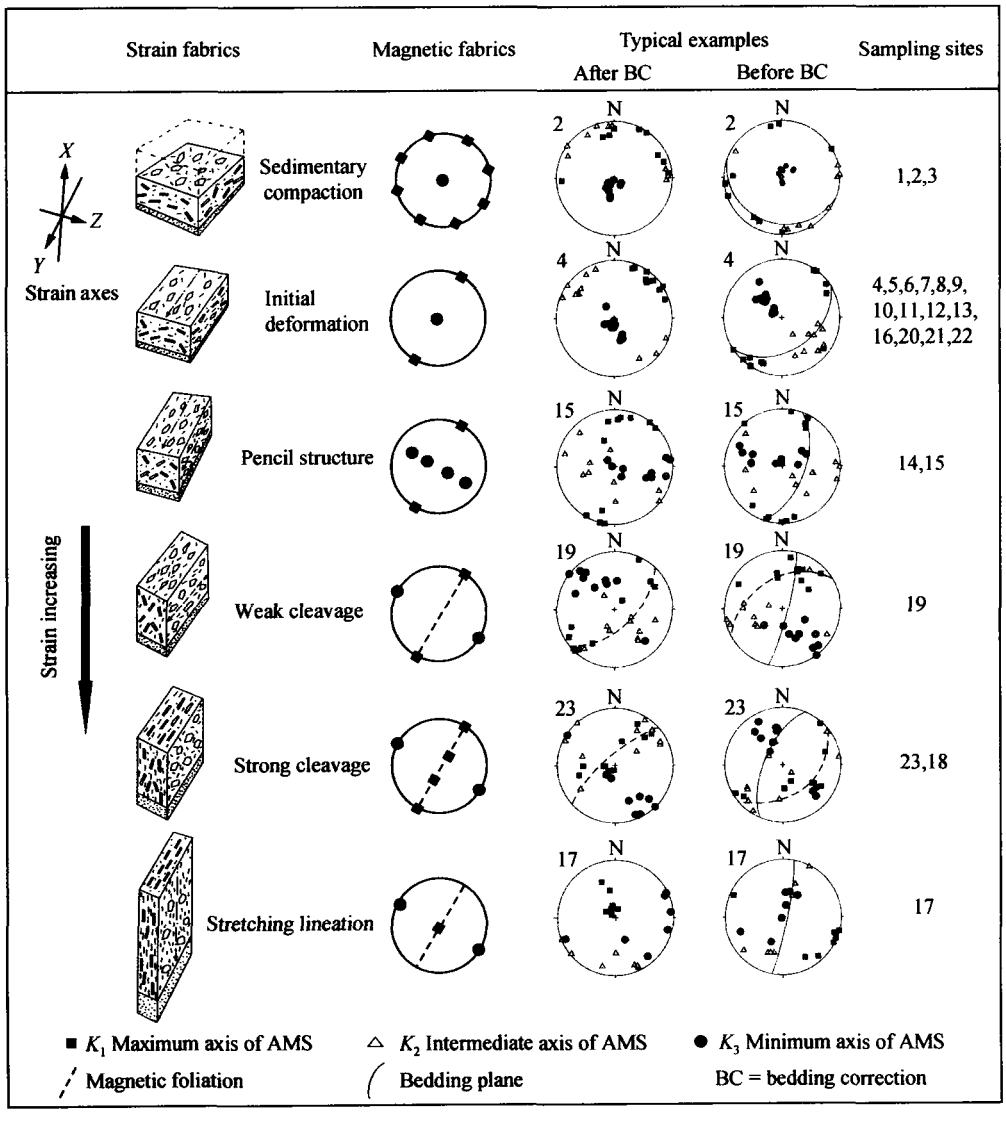

Fig. 4. Six elementary types of magnetic fabrics and its representing finite strains.

4 Finite strain analysis in fault-related fold

The development of a fault-related fold yields two kinds of strain in deformed sedimentary rocks. One kind of strain is pre-folding layer parallel shortening which has a property of pure shear deformation. In this deformation process, the magnetic fabric evolves from a layer parallel sedimentary fabric to an intermediate fabric with a strike-directing magnetic lineation, then to a tectonic fabric with a magnetic foliation normal to the bedding and shortening direction[2,24]. It is difficult to compute the magnitude of layer parallel shortening, while Hirt et al. (1995) and Sans et al. (1999) estimated that shortening amount can reach 20%[3,26]. Another kind of strain in fault-related folds has a property of simple shear which is controlled by the deforming mechanisms such as fault-bend folding[4], fault-propagation folding[5], trishear fault-propagation folding, etc[6]. The corresponding kinematic modeling has been used to predict the strain distribution at different structural domains and the result demonstrates that the magnetic foliation is oblique to the bedding as the results of simple shear deformation.

From the AMS investigation in Mingjiang section, we can see clearly that the finite strains reflected by the magnetic fabrics have obvious differences at different structural positions (Fig. 5). Firstly, we discuss the finite strain features reflected by the magnetic fabrics in the fault-bend fold (Baisha anticline). Three sites (1, 2, 3) locating at the footwall of the fault-bend fold have a sedimentary fabric, which means no noticeable finite strain appearing in footwall rocks. Sites 4 and 5 in the forelimb show the representative initial deformation fabric with bedding parallel magnetic foliation and fold-strike direction gathering K_1, which is also called an intermediate fabric by some scholars[24]. Eight sites (6, 7, 8, 9, 10, 11, 12 and 13) in the backlimb mainly display a weak initial deformation fabric, a transition fabric between the sedimentary fabric and initial deformation fabric, where K_1 and K_2 apart from each other while neither of them well-gathered. And only sites 7 and 13 present the typical features of the initial deformation fabric. As a comparison, the finite strains reflected by the magnetic fabrics in the forelimb of the Baisha fold are apparently stronger than those in the backlimb. It is important to denote that the initial deformation fabric appearing in the both limb of the fault-bed fold is the result of pure shear deformation of the pre-folding layer parallel shorting for its magnetic foliation is still parallel to the bedding[2,19,20,24]. The structural foliation caused by flexuring should be oblique to the bedding, just like the orientation of strain ellipsoid in the folded domain[7]. However, the fact that there are only the pre-folding finite strain and no folding strain in the Baisha fold indicates that finite strains in this fault-bend fold mainly take place under the pre-folding deformation of NW to NE (normal to the K_1 and K_3) compression.

Sites 14, 15, 16, 17, 18, 19 and 23 located at either the horizontal sedimentary layers or vertical ones in the footwall of this fault-propagation fold display strong magnetic fabrics and distinctly compose a triangular deformation area which is exactly consistent with the trishear deformation zone in the trishear fault-propagation fold[6,27,28] and means the finite strain developed in the process of fault-propagation folding (Fig.6). At site 23, a strong cleavage deformation is well presented by magnetic fabric investigation while there are no visible cleavages in the outcrop and hand specimens, denoting that AMS is highly sensitive to the weak deformation in sedimentary rocks. Although site 23 is situated at the backlimb of the Baisha fault-bend fold, its magnetic foliation trends southeast in contrast with the bedding trend. We also know that structural foliation caused by the interbedded sliding has the same dip direction with the bedding and has a bigger dip angle than that of the bedding. So we can infer that the fabric of site 23 formed before the development of Baisha fault-bend fold and was the result of the trishear deformation in the forelimb of the Bianbaigou fault-propagation fold. The magnetic fabric after bedding correction represents the actual structural strain of trishear deformation of site 23, which is characterized by the NW steep dipping magnetic foliation and SE plunging K_3 of the maximum compression stress (Fig. 6). Both site 14 at the horizontal layer and site 15 at the steep layer show the pencil structure fabrics which also have not been observed in the outcrop and indicate a NW to SE principal compressional stress. Site 16 has an initial deformation fabric because of the strong rock mechanic property. Site 17 at the vertical layer near the thrust fault is well marked by a bedding normal K_1 and a fabric characteristic of obvious magnetic lineation after bedding correction (Figs. 4—6). Site 18 at the slightly overturned layer shows a NW dipping

magnetic foliation which is oblique to the bedding with an angle of 20° and denotes a K_3 parallel (NW to SE direction) principal compressional stress. Like site 17, site 19 is also located at the vertical layer near the thrust fault and possesses a strong finite strain fabric where magnetic foliation is NW dipping and oblique to the bedding with large-angle. In the hanging wall of this fault-propagation fold, sites 20, 21 and 22 present an initial deformation fabric with bedding-normal K_3 and gradually aparted K_1 and K_2, which belong to the results of pre-folding layer parallel shortening deformation.

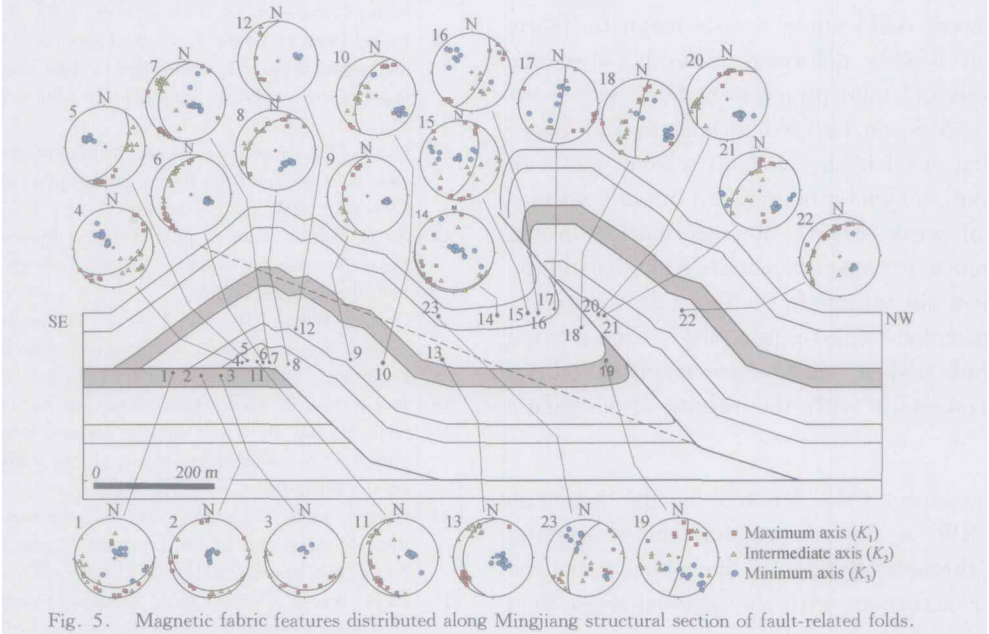

Fig. 5. Magnetic fabric features distributed along Mingjiang structural section of fault-related folds.

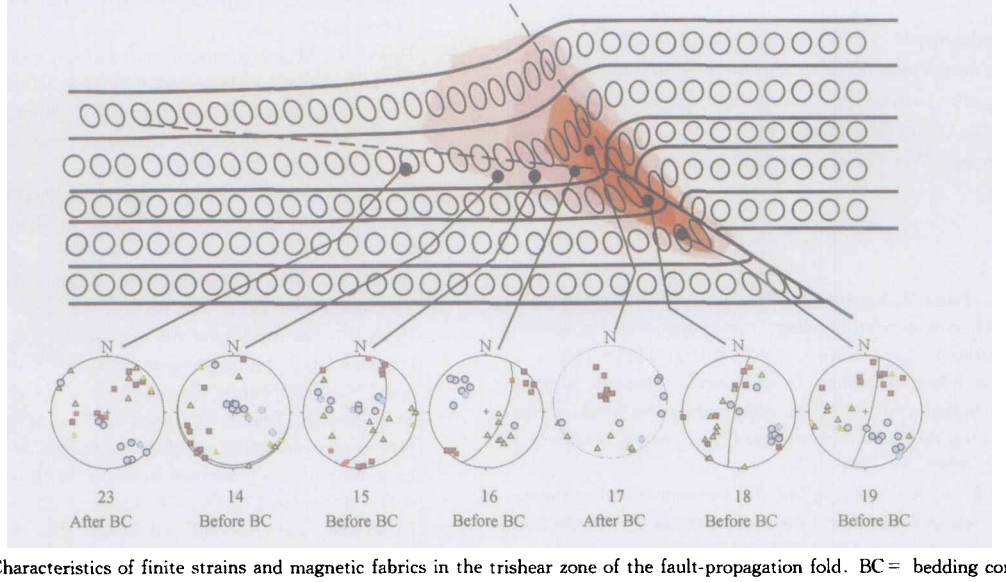

Fig. 6. Characteristics of finite strains and magnetic fabrics in the trishear zone of the fault-propagation fold. BC = bedding correction.

5 Discussion and conclusions

The AMS investigation along Mingjiang section denotes that magnetic fabrics can effectively reflect the finite strains in weakly deformed sedimentary rocks. Based on the developing sequence of strain fabrics in sedimentary rocks, six elementary types of magnetic fabric have been recognized and established, which indicates the relationship between the strain fabric and magnetic fabric. The AMS fabric is highly sensitive to the weak finite strain since the finite strain reflected by the magnetic fabric cannot be observed in filed outcrops and specimens.

The 14 sites of all sampling 23 sites in Mingjiang section having initial deformation fabrics means that

the finite strain in fault-related folds mainly developed in the pre-folding period and then the forthcoming folding process is only the decoupling sliding and rotation of the hanging walls of these folds. In our investigation there are no obvious strain fabrics caused by interbedded sliding in the fold limbs.

The present AMS study reveals magnetic fabric differences in weakly deformed rocks between the fault-bend fold and fault-propagation fold, which indicated that AMS can be used to analyze and verify the deforming mechanism of fault-related fold. In fault-bend fold, magnetic fabric is an initial deformation fabric of weak strain, the deformation in the forelimb is much stronger than that in the backlimb, and no finite strain appears in the footwall. However, in fault-propagation fold, finite strain is concentrated in the forelimb trishear zone where magnetic fabrics are highly consistent with the results of kinematic modeling.

Tectonic stress field denoted by the magnetic fabric is a NW to SE compressing and shortening which goes through all sites in the whole structural section and is accordant with the regional stress field of Longmenshan fold-thrust belt.

Acknowledgements We would like to thank Dr. Yang Zhenyu for his important helps in specimen sampling and measurement. We also thank CAS academician Jia Chengzao, professor Lu Huafu, Yang Shufeng, Chen Hanlin, Xiao Ancheng and Chief engineer Wei Guoqi for their assistance and advices for this work.

References

1 Aubourg C, Frizon de Lamotte D, Poisson A, et al. Magnetic fabrics and oblique ramp-related folding: a case study from the western Taurus (Turkey). J Struct Geol, 1997, 19(8): 1111—1120
2 Averbuch O, Frizon de Lamotte D and Kissel C. Magnetic fabric as a structural indicator of the deformation path within a fold thrust structure: a test case from the Corbières (NE Pyreness, France). J Struct Geol, 1992, 14: 461—474
3 Hirt A M, Evans K F and Engelder T. Correlation between magnetic anisotropy and fabric for Devonian shales on the Appalachian plateau. Tectonophysics, 1995, 247: 121—132
4 Suppe J. Geometry and kinematics of fault-bend folding. Am J Sci, 1983, 283: 684—721
5 Suppe J and Medwedeff DA. Geometry and kinematics of fault-propagation folding. Eclogae Geol, Helvetica 83, 1990: 409—454
6 Allmendinger RW. Inverse and forward numerical modeling of Trishear fault-propagation folds. Tectonics, 1998, 17: 640—656
7 Ramsay JG and Huber MI. The Techniques of Modern Structural Geology. Volume 1 Strain Analysis. London: Academic press, 1983
8 Elliott D. The motion of thrust sheets. J Geophys Res, 1976, 5: 949—955
9 Geiser PA. Mechanisms of thrust propagation: some examples and implications for the analysis of overthrust terranes. J Struct Geol, 1988, 10: 829—845
10 Mitra G. Strain variation in thrust sheets across the Sevier fold-and-thrust belt (Idaho-Utah-Wyoming): implications for section restoration and wedge taper evolution. J Struct Geol, 1994, 16: 585—602
11 Woodward NB, Gray DR and Spears DB. Including strain data in lalanced cross-sections. J Struct Geol, 1986, 8: 313—324
12 Lu H, Dong H, Deng X, et al. Types and origins of the thrusts and nappes in outer Longmenshan foreland basin. Journal of Nanjing University (Earth Sciences) (in Chinese), 1989, 4: 32—41
13 Luo Z. The dynamical model of the lithospheric evolution in Longmen Shan orogenic belt. Journal of Chengdu College of Geology (in Chinese), 1991, 18(1): 1—7
14 Xu Z, Hou L, Wang Z, et al. Orogenic Processes of the Songpan-Garzê Orogenic Belt of China. Beijing: Geological Publishing House (in Chinese), 1992, 190
15 Chen S, Wilson CJL, Luo Z, et al. The evolution of the western Sichuan foreland basin, southwestern China. Southeast Asian Earth Sci, 1994, 10(3/4): 159—168
16 Jia D, Chen Z, Jia C, et al. Structural features of the Longmen Shan fold and thrust belt and the western Sichuan foreland basin, central China. Geological Journal of China Universities (in Chinese), 2003, 9(3): 462—469
17 Chen Z, Jia D, Zhang Q, et al. Balanced cross-section analysis of the fold-thrust belt of the Longmen Mountains. Acta Geologica Sinica (in Chinese), 2005, 79(1): 38—45
18 Jia D, Wei G, Chen Z, et al. Longmen Shan fold-thrust belt and its relation to western Sichuan Basin in central China: new insights from hydrocarbon exploration. AAPG Bulletin, 2006, 90(9): 1425—1447
19 Hrouda F. Magnetic anisotropy of rocks and its application in geology and geophysics. Geophysical Surveys, 1982, 5: 37—82
20 Rochette P, Jackson M and Aubourg C. Rock magnetism and the interpretation of anisotropy of magnetic susceptibility. Rev Geophys, 1992, 30: 209—226
21 Borradaile GJ and Henry B. Tectonic applications of magnetic susceptibility and its anisotropy. Earth Sci Rev, 1997, 42: 49—93
22 Jelinek V. Characterization of the magnetic fabric of the rocks. Tectonophysics, 1981, 79: 63—67
23 Parés JP, van der Pluijm BA and Dinarès-Turell J. Evolution of magnetic fabric during incipient deformation of mudrocks (Pyreness, Northern Spain). Tectonophysics, 1999, 307: 1—14
24 Saint-Bezar B, Hebert RL, Aubourg C, et al. Magnetic fabric and petrography investigation of hematite-bearing sandstones within ramp-related folds: examples from the South Atlas Front (Morocco). J Struct Geol, 2002, 24: 1507—1520
25 Evans MA, Lewchuk MT and Elmore RD. Strain partitioning of deformation mechanism in limestone: examining the relationship of strain and anisotropy of magnetic susceptibility (AMS). J Struct Geol, 2003, 25: 1525—1549
26 Sans M, Vergès J, Gomis JM, et al. Layer parallel shorting in salt-detached folds: constraints on cross-section restoration. Thrust Tectonics 99, Royal Holloway Universuty of London, 26—29 April 1999, Volume abstract, 321—324
27 Erslev EA. Trishear fault-propagation folding. Geology, 1991, 19: 617—620
28 Zehnder AT and Allmendinger RW. Velocity field for the trishear model. J Struct Geol, 2000, 22: 1009—1014